Integration of PbS quantum dot photodiodes on silicon for NIR imaging

Epimitheas Georgitzikis, Pawel E. Malinowski, Yunlong Li, Jorick Maes, Luis Moreno Hagelsieb, Stefano Guerrieri, Zeger Hens, Paul Heremans and David Cheyns

***Abstract*—Colloidal quantum dots based on lead sulfide (PbS) are very attractive materials for the realization of novel image sensors. They offer low cost synthesis, compatibility with a variety of substrates and processing on large area. The tunable band gap enables selective light detection from the visible wavelengths up to the short-wave-infrared (SWIR). This work describes the roadmap towards the integration of quantum dot photodiodes (QDPD) on top of a Si based CMOS read-out circuit. Photodiodes using an n-p junction architecture are fabricated on Si substrates, showing a dark current of 30 nA/cm^2 at -1 V reverse bias, EQE above 20% and specific detectivity above 10^{12} cm Hz$^{1/2}$ W^{-1} at the wavelength of 940 nm. Efficiency is improved by reducing absorption in the top contact through optical design. Furthermore, photolithographic patterning of the thin-film stack is introduced for the first time, showing the feasibility of pixel pitches down to 40 µm, opening the way towards high resolution monolithic infrared imagers and the incorporation of infrared and visible sensitive pixels side by side.**

***Index Terms*— infrared image sensors, infrared imaging, photodetectors, PbS QDs, quantum dots, thin film sensors, CMOS integration.**

I. Introduction

DEMAND for near-infrared (NIR) imaging is growing. Surveillance, optical tomography, process monitoring, LiDAR or Advanced Driver Assistance Systems and eye/head tracking all need imaging at low light levels, beyond visible wavelengths and with specific illumination sources. As the absorption of Si sharply decreases at wavelengths above 900 nm, state-of-the-art infrared (IR) imagers use silicon circuitry for pixel readout in combination with flip-chip bonded III-V materials [1]–[4]. Even though these hybrid detectors can offer great performance, they are characterized by a significantly high fabrication cost and low throughput. Typically, an InGaAs or HgCdTe absorber is used. This requires high temperature epitaxial growth on small wafer sizes. The solder bump process used to connect the absorber with the CMOS read-out circuit (ROIC) which restricts the achievable pixel resolution to 10 µm [5]. Taking these points into consideration, the development of low cost and high resolution infrared photodetectors can become a major driver of growth for the IR imaging.

Thin-film materials can overcome the aforementioned restrictions as they can be monolithically integrated on top of a Si-based CMOS ROIC using solution processing deposition techniques [6]. In this way, there is potentially no limiting factor in the achievable resolution (pixel pitch is defined by the ROIC) and full wafer level processing can be enabled. Previous reports have already demonstrated image sensors with thin-film materials using organic absorbers [7]–[10], while over the last years there have been significant advances achieved in the integration of these films on CMOS with good performance and pixel size of as low as 0.9 µm [11], [12] (Fig. 1). A similar concept can be envisaged for IR sensors, for which colloidal quantum dots (QDs) are ideal candidates because of the quantum effect bandgap tuning that allows the detection to shift to a wide range of wavelengths from the visible up to SWIR (Fig. 2) [13], [14]. QDs based on lead-sulfide (PbS) have acquired a lot of interest in the last years due to the ease of synthesis and processing [15]. Taking advantage of the large exciton Bohr radius of the PbS (18 nm) the band gap of the QDs can be tuned depending on the nanocrystal diameter to cover the entire near-infrared and short-wave-infrared spectrum [16]. Most common sizes in literature vary between 2.8 nm (absorption peak $\lambda = 800$ nm) to 8 nm (absorption peak $\lambda = 1800$ nm) while successful synthesis of PbS QDs with diameter up to 10 nm corresponding to absorption peak wavelengths of 2100 nm has been also reported [17]–[19]. At the same time a variety of devices targeting different wavelengths in the NIR and SWIR spectrum have been shown using different configurations and stacks [19]–[24]. These devices are fabricated on bottom illuminated large size passive pixels on glass substrates with

This paragraph of the first footnote will contain the date on which you submitted your paper for review. An earlier version of this paper was presented at the IEEE Sensors 2018 and was published in its Proceedings https://ieeexplore.ieee.org/document/8589515.

Epimitheas Georgitzikis and Paul Heremans are with imec Kapeldreef 75, B-3001 Leuven, Belgium and also with ESAT, Katholieke Universiteit Leuven, Kasteelpark Arenberg 10, B-3001 Leuven, Belgium (e-mail: Epimitheas.Georgitzikis@imec.be; Paul.Heremans@imec.be).

Pawel E. Malinowski, Yunlong Li, Luis Moreno Hagelsieb, Stefano Guerrieri and David Cheyns are with imec Kapeldreef 75, B-3001 Leuven, Belgium (e-mail: Pawel.Malinowski@imec.be; Yunlong.Li@imec.be; Luis.MorenoHagelsieb@imec.be; Stefano.Guerrieri@imec.be; David.Cheyns@imec.be).

Jorick Maes and Zeger Hens are with Physics and Chemistry of Nanostructures, Ghent University, Krijgslaan 281-S3, B-9000 Ghent, Belgium and also with Center for Nano- and Biophotonics (NB-Photonics), Ghent University, B-9000 Ghent, Belgium (e-mail: jorick.maes@ugent.be; zeger.hens@ugent.be).

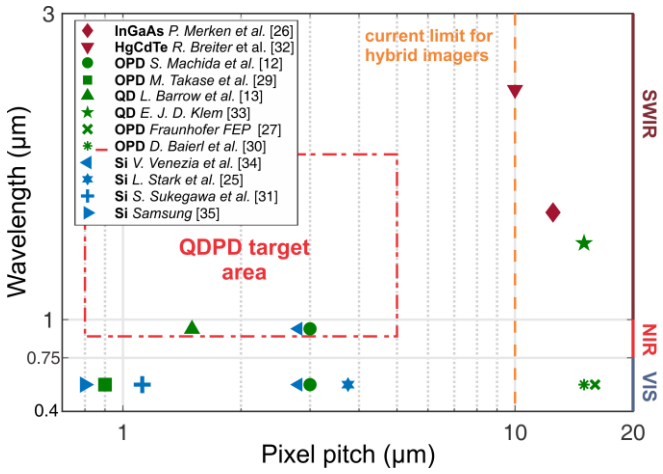

Fig. 1.Pixel pitches reported for different absorption wavelength regions and comparison of the imagers using thin-film absorbers on CMOS with the state of the art Si absorbers and hybrid imagers using InGaAs and MCT (HgCdTe) on CMOS [12], [13], [25]–[35].

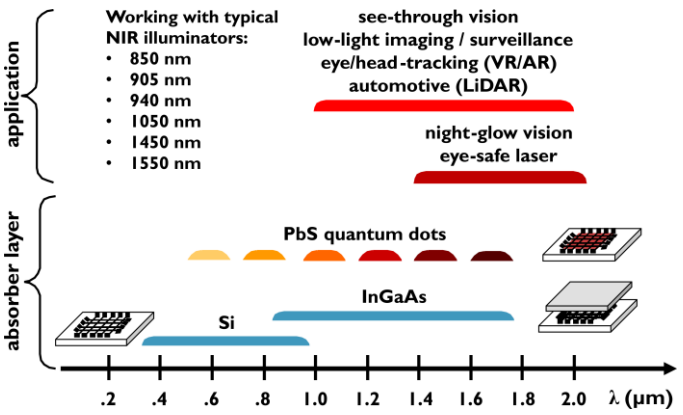

Fig. 2. NIR spectrum applications and positioning of QDPD against state of the art absorbers.

ITO contacts and manual-mechanical scrubbing used for the cleaning of the contact pads. Here, we report QDPD on Si substrates developed for CMOS integration with a NIR absorption peak at 940 nm. This wavelength is of particular interest due to the water absorption window in the atmosphere and compatibility with the standard NIR illumination sources. High performance devices with low dark current and pixel size down to 20 µm are demonstrated. Then, the devices are further optimized for integration by enhancing their optical properties. Next, photolithographic patterning of the thin-film stack is introduced, opening the way for high resolution monolithic IR sensors or even the integration of additional photodiodes next to conventional Si pixels, hence extending the sensitivity spectrum (Fig 3).

II. Experimental

A. PbS QDs

The PbS QDs were synthesized by a previously published method [17], making use of lead oleate and N-(3,5-bis(trifluoromethylphenyl))-N'-phenylthiourea. After four purification cycles the QDs are dispersed in n-octane for the device fabrication. The first excitonic peak of the QD dispersion is positioned at 901 nm which corresponds to a QD diameter of 3.23 nm according to SAXS-calibrated sizing curves [36].

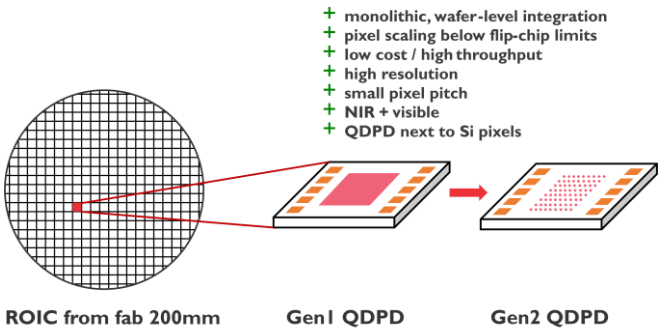

Fig. 3. Integration of QDPD on Si. From 200 mm wafer to monolithic NIR imager in two configurations: photolithographic patterning of the TFPD stack per active area (Gen1) and per pixel (Gen2).

B. Device fabrication

The photodiode is created in an n-p junction architecture. Si/SiO_2 substrates are used with a metal bottom contact to imitate the surface and interconnects of a CMOS read-out-circuit (ROIC). TiN is used as the bottom contact due to its compatibility with the CMOS process flow and also for its high reflectivity in the infrared range. The thin QD film (100 – 200 nm) is deposited by spin coating in a layer-by-layer approach between an electron transport layer (ETL) and an organic hole transport layer (HTL). A few drops of QD solution are deposited on the substrate which is then spun to dry. Subsequently, the substrate is covered by a solution of thiols in acetonitrile. The thiols will replace the original passivating ligands (oleic acid) enabling carrier transport between adjacent nanoparticles. The described process leads to the formation of one QD layer with thickness of approximately 15 nm. This PbS film deposition and ligand exchange procedure is repeated until the target thickness is achieved. For the ETL, an n-type

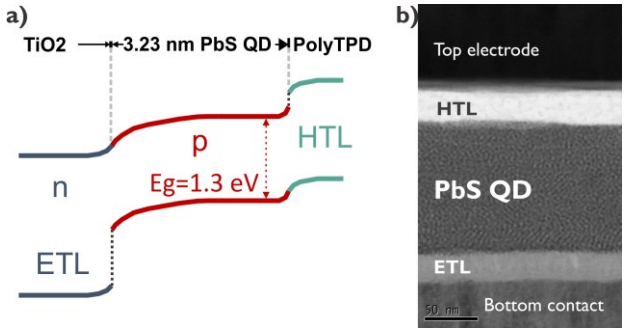

Fig. 4. QD photodiode stack. Band diagram of the n-p junction and annular bright-field scanning transmission electron microscopy (ABF-STEM) image of the stack in cross-section. The QD film reveals the arrangement of the nanoparticles in a lattice separated by the ligands.

metal oxide is used to form the junction with the QD layer. Fig. 4a shows the band diagram of the fabricated detector. The stack is finished with a semi-transparent contact allowing top-side illumination. Either thermally evaporated Ag or a sputtered ITO are used. The complete photodiode stack is shown in a transmission electron microscopy (TEM) cross-section image in Fig. 4b revealing the lattice formation of the QDs separated by their ligands. The substrate consists of many passive pixels with sizes ranging from 20×20 µm^2 to 2×2 mm^2. The size of the pixel is defined accurately by an inorganic edge cover layer (ECL) which excludes the contribution of the fanout structure to the device area, in a single metallization fanout scheme.

C. Device characterization

The current voltage characteristics of the photodiodes under dark and IR illumination are measured in a dark box using an Agilent 4155C Semiconductor Parameter Analyzer.

The speed measurements are performed in a dark box using an IR LED with rise and fall time of 100 ns. For the measurement the LED gives pulses of 1 ms and the photodiode output is measured using a Stanford Research SR830 lock-in amplifier and an oscilloscope.

The EQE and responsivity (R) measurements are performed using a Bentham PV300 Spectral Response system. A light beam from a Xenon/Quartz halogen source is coupled into a Bentham TMc300 single monochromator, giving a coverage over the spectral range of 300-2500nm. The reflection and transmission measurements are executed using an integration sphere.

III. Results and Discussion

A. QDPD performance

One of the figures-of-merit for an efficient photodetector and for its incorporation as an imager pixel, is the dark current (I_d) under reverse bias operation. The current-voltage (I-V) curve of the developed devices (Fig. 5a) shows a low dark current of 29 nA/cm^2 at an applied reverse bias of -1 V, which is among the lowest dark current values reported in the literature. The photo-response of the test devices is measured using an infrared LED with emission at 940 nm. For a light intensity of 5 mW/cm^2, a photocurrent of 1.9 mA/cm^2 at -1 V is measured, corresponding to a photocurrent-to-dark current ratio of 90 dB. Furthermore, linear scaling of the diode current with the pixel size is observed both under dark conditions and under illumination with a 940 nm NIR LED, indicating the feasibility of high resolution image sensors (Fig. 5b). Fig. 5c shows the linear scaling of the photocurrent for increasing illumination intensity at 940 nm.

A second photodetector figure of merit is the responsivity R (measured in A/W), expressing the ratio between the photocurrent and the flux of the incident light. The responsivity can be directly translated to the external quantum efficiency (EQE). Using the responsivity and assuming that the device noise is dominated by the dark current in our diodes-we derive the specific detectivity (D^*) which is widely used to characterize the performance of infrared photodiodes and is given by:

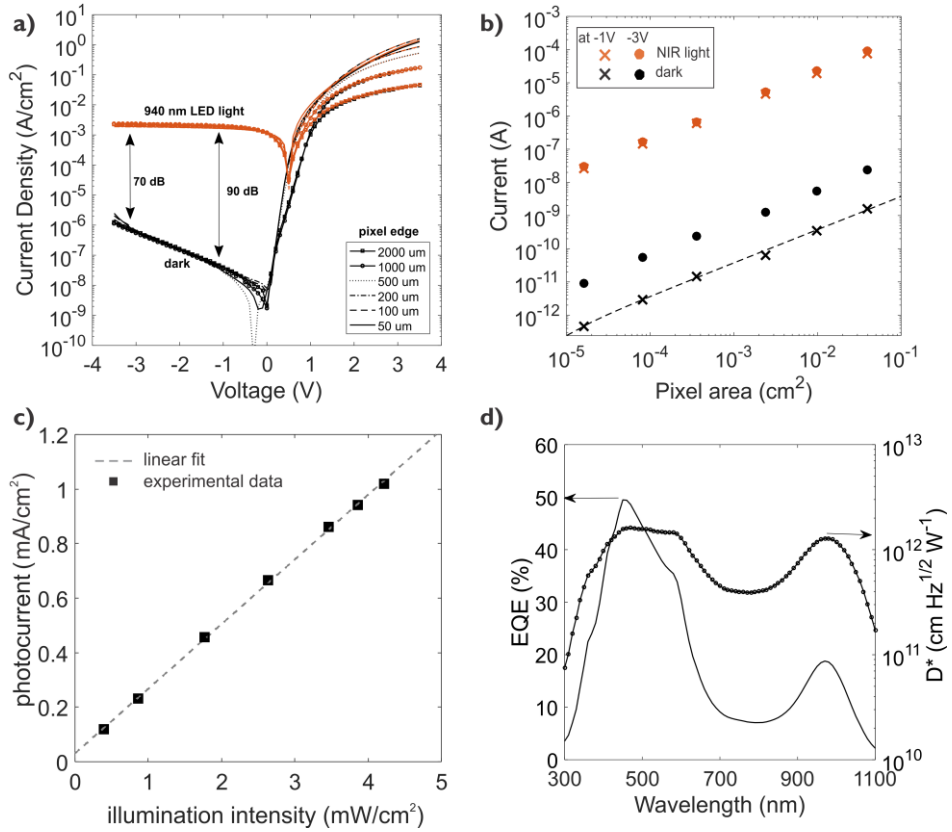

Fig. 5. QDPD characterization: a) I-V characteristics under dark conditions and under illumination from a 940 nm LED and intensity of 5 mW/cm^2 b) linearity of photocurrent and dark current versus pixel area c) linearity of the photocurrent for different illumination power at 3 V reverse bias and d) the external quantum efficiency (EQE) at 1 V reverse bias of the top illuminated photodiode on silicon and the specific detectivity considering as main noise source the shot noise.

$$D^*(\lambda) = R(\lambda)\cdot A^{1/2}\cdot(2qI_d)^{-1/2} \quad (1)$$

where A is the device active area, q the electron charge and I_d the dark current [22], [37]. Our top illuminated devices achieve an EQE of 21 % at 940 nm at bias of -1 V. Taking the dark current as the major noise component, the obtained specific detectivity surpasses 10^{12} cm Hz^{½} W^{-1} (Fig. 5d). For the realization of the best possible efficiency for the stack, an optical optimization was employed and will be discussed in the next paragraph.

To characterize the temporal photo-response, the devices are illuminated with a pulsed light emitted from an LED source with a peak at 940 nm while their output is sampled using an oscilloscope. Rise (10% to 90% of the photogenerated signal) and fall (90% to 10% of the photogenerated signal) times of 57 μs and 86 μs, respectively, are obtained as shown in Fig. 6. Such performance corresponds to bandwidth over 10 kHz and is sufficient for basic imaging applications. The above analysis showcases the feasibility of fabricating IR image sensors with thin-film materials. Still, the performance of the QDPDs is significantly lower than their III-V based competitors. This is balanced by the ease and corresponding lower cost of fabrication and the absorption tunability. Additionally, latest reports showcase solar cells using PbS QD achieving EQE

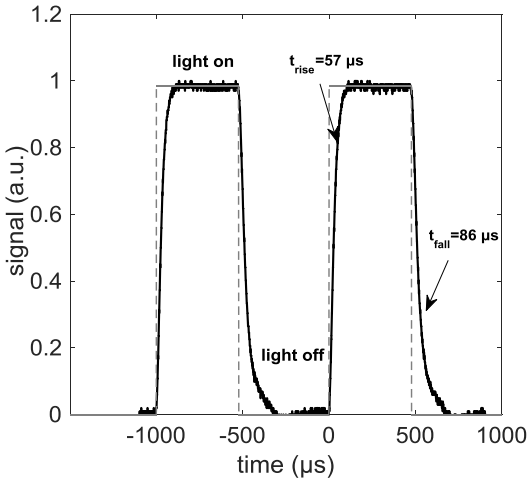

Fig. 6. Transient photo-response of a quantum dot photodiode.

values of 80% in the NIR region [38]. Even though these configurations sacrifice dark current performance for efficient solar light harvesting, we expect that an optimized photodetector stack can reach EQE of 60%.

B. Optical design

While the electrical design is fundamental in the formation of a good photodiode, a proper optical design can significantly enhance its quantum efficiency. Specifically, in devices with layer thicknesses that are in the range of the wavelength of the incident light, even small changes in the layer thicknesses can change radically the way that the light propagates through the layers. Taking advantage of this effect by forming optical cavities can boost the light absorption. We have used a similar concept in our previous work [39], in order to enhance the photo-response of SWIR quantum dot photodetectors for bottom illumination. In bottom illuminated devices typically, metals such as Ag or Au are used as top contacts. However, these materials have very low transparency. Thus, for top illumination the main challenge lies in finding suitable metals for both the top and bottom contact. A transparent top contact is crucial while a reflective bottom contact can boost the light harvesting. TiN proved to be a satisfactory candidate for the bottom electrode (reflection > 60% in the IR) while an optimized ITO top contact can provide the required transparency Fig. 7a. To demonstrate the impact of the top contact we have fabricated devices on Si substrate using the same ETL/QD/HTL stack and different top contact. Fig. 7b shows the difference in the measured EQE of two devices, one having a 10 nm Ag low transparency anode and the other an optimized ITO for maximum performance at 940 nm. The latest achieves 2.5 times higher photo-response even though they use the same absorber thickness.

In order to achieve this maximum EQE we build an optical model that can accurately simulate the optical behavior of the stack. The model takes as input the complex refractive index $\underline{n} = n + ik$ of all the materials used in the QDPD.as input (where n is the refractive index and k is the extinction coefficient). These values are obtained through ellipsometry in combination with reflection and transmission measurements [39]. Then, the transfer matrix algorithm is used to analyze the propagation of the light through each layer of our stack and calculate the total electric field E inside the system. By simulating different thicknesses of the photodiode layers we attempt to create a constructive optical interference that will maximize the E. The electric field at each wavelength can be easily converted to the number of absorbed photons G:

$$G = 2\pi\cdot\varepsilon\cdot(h)^{-1}\cdot n\cdot k\cdot|E|^2 \quad (2)$$

where ε is the material permittivity, h the plank constant. Assuming that all the absorbed photos are contributing to the photocurrent we can calculate the maximum expected EQE [40], [41].

As a first step, the EQE at the wavelength of interest (940 nm here) with varying thickness of the transport layers is simulated while the thicknesses of QD film and the top contact remain constant. The results are shown in Fig. 8a indicating that the optimal thickness for the ETL and the HTL are in the vicinity of 50 nm. Using these values, we proceed by simulating the

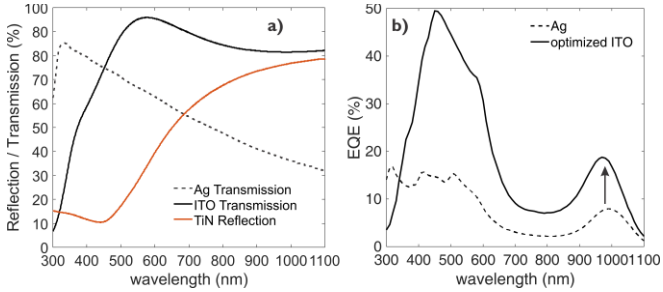

Fig. 7. Material selection for the photodiode contacts. a) Transmission of 10 nm Ag, 140 nm of ITO and reflection of TiN on glass substrate for top illumination; b) Improvement in the external quantum efficiency of the photodiode when passing from a low transparency standard metallic top contact to an optimized anode. EQE measured at 1 V reverse bias.

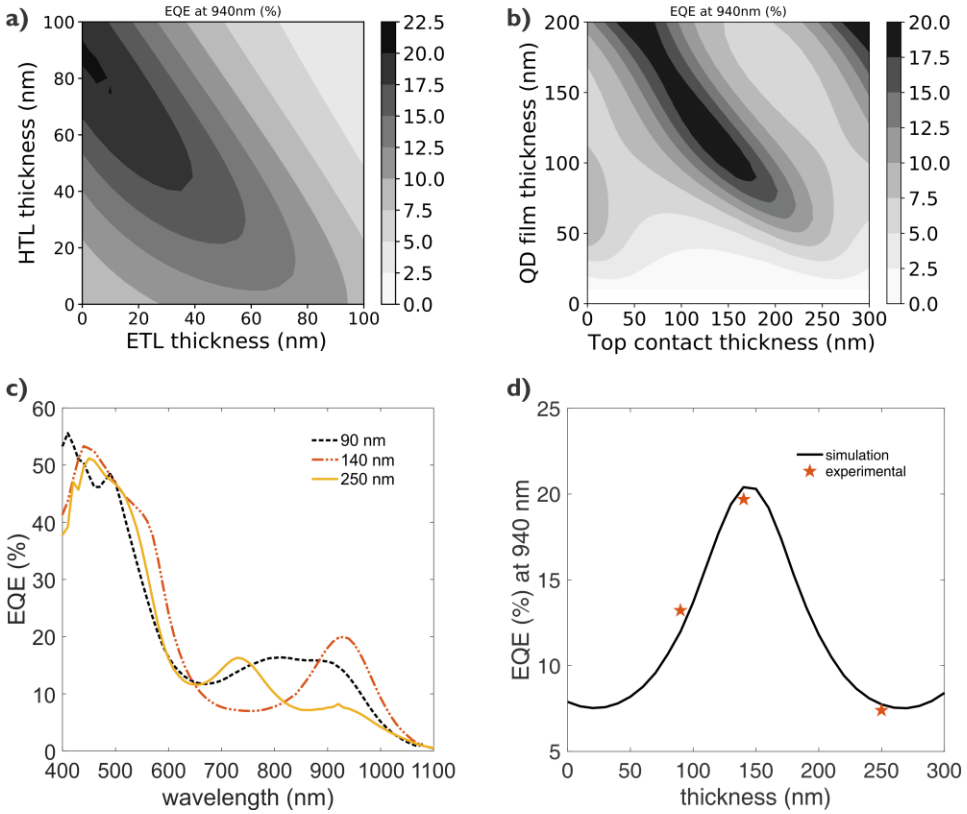

Fig. 8. Optical simulations using the developed QDPD model for varying thickness of a) the HTL and ETL and b) for varying QD film and top contact thicknesses. Experimental verification in c) for three identical devices with only variation the top contact thickness. The predicted shift of the optical cavity depending on the anode thickness is demonstrated. The maximum EQE is obtained for 140 nm contact in good agreement with the simulations d).

efficiency while varying the QD layer and the top contact thickness. From this simulation (Fig. 8b), we obtain peak EQE values for QD thickness between 100 to 150 nm with top contact thicknesses of 100 to 175 nm. In order to verify the model, we build photodiodes using the findings of the simulation phase. For the ETL and HTL, the aforementioned values are used while keeping the QD film thickness as 120 nm taking into account the limited diffusion length of the generated carriers. Fig. 8c shows the EQE results for the fabricated photodiodes for 3 different thicknesses of the top contact. It is clear, that only by changing the thickness of one layer, the optical response of the QDPD changes significantly as the formed optical cavity shifts. For the 90 nm contact, two peaks are formed at λ=800 nm and λ=900 nm while for the 250 nm contact, a cavity is formed at λ=730 nm. Simulations predict that the use of a top contact of 140 nm creates an optical cavity for λ=940 nm (Fig. 8b) and indeed this is proven by the EQE measurement which demonstrates a single maximum peak around λ=940 nm. Finally, Fig. 8d shows a one dimensional simulation of the quantum efficiency at the target wavelength while varying the top contact thickness side-by-side with the experimental results. It is clear that the device data accurately follows the modeling trends. In summary, the developed model accurately predicts the optical behavior of a QD photodiode. Via a proper selection of stack layers and a fine-tuning of the layer thicknesses we manage to boost the EQE from 8% to 20% at the target wavelength even when using a very thin and weak absorber.

C. *Integration aspects*

A high performance demonstration is a prerequisite for the final establishment of this technology. Nevertheless, the next step is the integration of a QDPD on a Si-based ROIC and preferably within a fab compatible process flow. Still, the integration route has a lot of challenges and restrictions to be overcome before making the quantum dot photodiodes a viable option for the next generation IR imagers. These challenges lie in the limited choice of contact materials and the efficient delivery of light to the photoactive layer through a semi-transparent top contact, while photolithographic patterning is a necessity towards the formation of high resolution pixel arrays. In the previous paragraph we discussed thoroughly the efficient light harvesting in a top-illuminated QD photodiode on silicon. In this section, we will focus on the photolithographic patterning of the QDPD stack. Being able to pattern thin-film materials that are deposited on the ROIC has significant advantages. While the most common practice during the development of a solution processed thin-film photodiode is manual scrubbing for the cleaning of the contact pads, this method is not accurate enough to be applied in small structures and it cannot be used for high-volume manufacturing. Photolithography on the other hand, is a method commonly used in fab process flows and can offer high accuracy in order to create even higher resolution pixel arrays.

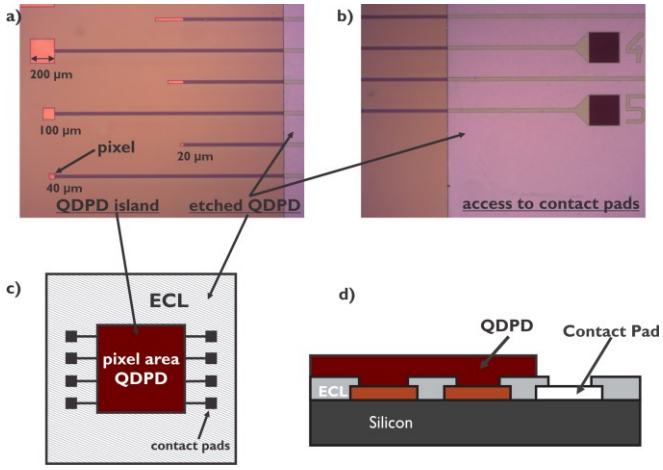

Fig. 9 Photolithographic patterning of the QDPD stack: a) a large island that covers the pixel area is formed while b) the material covering the contact pads is etched away allowing bonding and packaging. c) shows a top view schematic of the pattering performed and d) illustrates the same in cross-section.

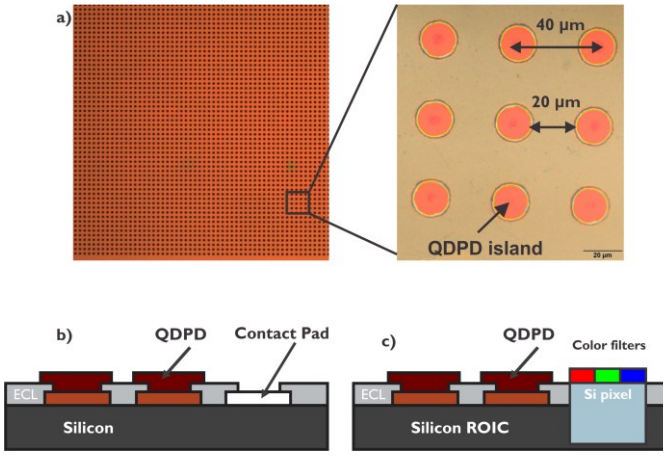

Fig. 11. A high resolution pixel array is created by photolithographic pattering forming isolated pixels of 20 µm diameter and 40 µm pitch: a) microscope image of the achieved patterning that is illustrated in cross-section in b); and c) gives a schematic of devices with isolated hi-resolution QDPD islands next to Si pixels.

In this work, by modifying a method adopted from literature [42], we demonstrate for the first time PbS QD photodetectors with a photolithography-patterned pixel stack. As a first step, the QDPD is patterned in order to create a large island that covers the entire focal plane area while leaving the contact pads uncovered. This is illustrated in the schematic of Fig. 9a-b, with a microscope image at the edge of the patterned area. Pixels of different sizes (down to 20 µm) are covered by the QDPD island whereas the contact pads have been exposed enabling the bonding and packaging of the device (schematic cross-section shown in Fig. 9d). Using this method, the pixel pitch is solely defined by the ROIC, so sub-micron pitches close to those in state-of-the-art silicon imagers can be considered. After the patterning step, the photodetector performance remains the same (dark/photocurrent and EQE values are maintained). In order to check the compatibility with the standard imager fabrication procedure, the developed sample was diced and packaged. Fig. 10 provides an image of a packaged QDPD detector and a schematic cross-section of the fabricated stack.

Going a step further, the feasibility of creating high resolution QDPD pixel arrays is tested. This is performed on Si/SiO_2 substrates without bottom contacts. Fig. 11 shows the results of such a patterning process. A pixel array is successfully created with 40 µm pixel pitch. The pixel isolation not only cancels potential cross-talk between adjacent pixels

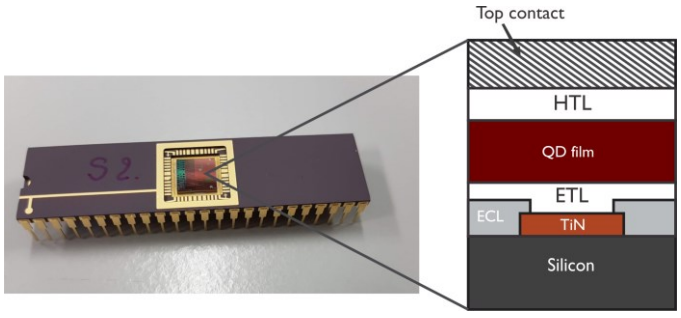

Fig. 10. Packaged sensor (left) and a schematic cross section (right) of the photodiode stack on Si substrate.

but also opens the way for new integration concepts. One of those is presented in the schematic of Fig. 11d. Quantum dot photodiode pixels can be developed on top of a CMOS imager and next to standard pinned Si photodiode pixels, extending the sensitivity range of the imager to NIR in a low-cost and efficient way.

IV. Conclusions

Thin-film photodetectors using PbS quantum dots as IR absorber provide a low-cost alternative to III-V materials. Monolithic heterogeneous integration enables further downscaling of the pixel size (below 10 µm, currently achievable only for CMOS imagers), cross-talk reduction and multispectral arrays. Here, we demonstrate essential building blocks for integration of the QDPD on substrates with a metal bottom contact layer to imitate the surface and interconnects of a CMOS ROIC. Speeds of 57 µs and 86 µs for rise and fall time respectively, a dark current of 29 nA/cm^2 and an EQE above 20% at 940 nm are demonstrated. From an integration aspect, the top illuminated stack is electrically and optically optimized for fabrication on silicon. Photolithographic patterning of the QDPD stack is introduced and the feasibility of high resolution pixels arrays is shown, opening the way for a new generation of monolithic infrared image sensors.

Acknowledgment

The results reported in this paper have been realized with the funding of Agentschap Innoveren & Ondernemen (VLAIO) in the framework of project MIRIS (IWT/150029).

References

[1] A. Rogalski, “Infrared detectors: Status and trends,” *Prog. Quantum Electron.*, vol. 27, no. 2–3, pp. 59–210, 2003.

[2] J. Barton, R. Cannata, and S. Petronio, “InGaAs NIR focal plane arrays for imaging and DWDM applications,” *Proc. SPIE*, 2002.

[3] J. John, L. Zimmermann, S. Nemeth, T. Colin, P. Merken, and S. Borghs, “Extended InGaAs on GaAs Detectors for SWIR Linear Sensors,” *Technology*, 2001.

[4] K. Lee *et al.*, “Band alignment of InGaZnO/Si interface by hard x-ray photoelectron spectroscopy,” *J. Appl. Phys.*, vol. 112, no. 3, p.

033713, 2012.
[5] J. Jiang, S. Tsao, T. O'Sullivan, M. Razeghi, and G. J. Brown, "Fabrication of indium bumps for hybrid infrared focal plane array applications," *Infrared Phys. Technol.*, vol. 45, no. 2, pp. 143–151, 2004.
[6] P. Malinowski *et al.*, "Thin-Film Quantum Dot Photodiode for Monolithic Infrared Image Sensors," *Sensors*, vol. 17, no. 12, p. 2867, Dec. 2017.
[7] G. Yu, J. Wang, J. McElvain, and A. J. Heeger, "Large-Area, Full-Color Image Sensors Made with Semiconducting Polymers," *Adv. Mater.*, vol. 10, no. 17, pp. 1431–1434, Dec. 1998.
[8] S. Tedde, E. S. Zaus, J. Fürst, D. Henseler, and P. Lugli, "Active pixel concept combined with organic photodiode for imaging devices," *IEEE Electron Device Lett.*, vol. 28, no. 10, pp. 893–895, 2007.
[9] T. Someya *et al.*, "Integration of Organic FETs With Organic Photodiodes for a Large Area , Flexible , and," *Electron Devices, IEEE Trans.*, vol. 52, no. 11, pp. 2502–2511, 2005.
[10] P. E. Malinowski *et al.*, "Fully Organic Integrated Arrays on Flexible Substrates for X-Ray Imaging," in *IISW 2013*, 2013.
[11] M. Takase, Y. Miyake, T. Yamada, T. Tamaki, M. Murakami, and Y. Inoue, "First demonstration of 0.9 µm pixel global shutter operation by novel charge control in organic photoconductive film," in *2015 IEEE International Electron Devices Meeting (IEDM)*, 2015, pp. 30.2.1-30.2.4.
[12] S. Machida *et al.*, "A 2.1-Mpixel Organic Film-Stacked RGB-IR Image Sensor With Electrically Controllable IR Sensitivity," *IEEE J. Solid-State Circuits*, vol. 53, no. 1, pp. 229–235, Jan. 2018.
[13] L. Barrow *et al.*, "A QuantumFilm based QuadVGA 1.5µm pixel image sensor with over 40% QE at 940 nm for actively illuminated applications," in *IISW 2017*.
[14] Z. Hens and I. Moreels, "Light absorption by colloidal semiconductor quantum dots," *J. Mater. Chem.*, vol. 22, no. 21, p. 10406, 2012.
[15] A. Shrestha, M. Batmunkh, A. Tricoli, S. Dai, and S. Z. Qiao, "Recent Advance in Near-Infrared Active Lead Chalcogenide Quantum Dots: Preparation, Post-Synthesis Ligand Exchange and Applications in Solar Cells," *Angew. Chemie Int. Ed.*, 2018.
[16] I. Moreels *et al.*, "Size-dependent optical properties of colloidal PbS quantum dots," *ACS Nano*, vol. 3, no. 10, pp. 3023–3030, 2009.
[17] M. P. Hendricks, M. P. Campos, G. T. Cleveland, I. Jen-La Plante, and J. S. Owen, "A tunable library of substituted thiourea precursors to metal sulfide nanocrystals," *Science (80-.).*, vol. 348, no. 6240, pp. 1226–1230, Jun. 2015.
[18] M. A. Hines and G. D. Scholes, "Colloidal PbS Nanocrystals with Size-Tunable Near-Infrared Emission: Observation of Post-Synthesis Self-Narrowing of the Particle Size Distribution," *Adv. Mater.*, 2003.
[19] J. W. Lee, D. Y. Kim, S. Baek, H. Yu, and F. So, "Inorganic UV-Visible-SWIR Broadband Photodetector Based on Monodisperse PbS Nanocrystals," *Small*, vol. 12, no. 10, pp. 1328–1333, Mar. 2016.
[20] J. P. Clifford, G. Konstantatos, K. W. Johnston, S. Hoogland, L. Levina, and E. H. Sargent, "Fast, sensitive and spectrally tuneable colloidal-quantum-dot photodetectors," *Nat. Nanotechnol.*, vol. 4, no. 1, pp. 40–44, 2009.
[21] T. Rauch *et al.*, "Near-infrared imaging with quantum-dot-sensitized organic photodiodes," *Nat. Photonics*, vol. 3, no. 6, pp. 332–336, 2009.
[22] B. N. Pal, I. Robel, A. Mohite, R. Laocharoensuk, D. J. Werder, and V. I. Klimov, "High-Sensitivity p-n junction photodiodes based on Pbs nanocrystal quantum dots," *Adv. Funct. Mater.*, vol. 22, no. 8, pp. 1741–1748, 2012.
[23] J. Gao, S. C. Nguyen, N. D. Bronstein, and A. P. Alivisatos, "Solution-Processed, High-Speed, and High-Quantum-Efficiency Quantum Dot Infrared Photodetectors," *ACS Photonics*, vol. 3, no. 7, pp. 1217–1222, 2016.
[24] E. Lhuillier *et al.*, "Infrared Photodetection Based on Colloidal Quantum-Dot Films with High Mobility and Optical Absorption up to THz," *Nano Lett.*, vol. 16, no. 2, pp. 1282–1286, 2016.
[25] L. Stark, J. M. Raynor, F. Lalanne, and R. K. Henderson, "Back-illuminated voltage-domain global shutter CMOS image sensor with 3.75µm pixels and dual in-pixel storage nodes," *Dig. Tech. Pap. - Symp. VLSI Technol.*, vol. 2016-Septe, pp. 1–2, 2016.
[26] P. Merken, R. M. Vinella, K. Wouters, V. Vervenne, and D. De Gaspari, "A 400 KHz line rate 2048-pixel stitched SWIR linear array," in *Infrared Technology and Applications XLII*, 2016, vol. 9819, no. May 2018, p. 981907.
[27] Fraunhofer FEP, "CMOS-based microdisplays, imager, and sensors enhanced by OLED/OPD integration," in *SEMI European Imaging & Sensors Summit 2017*, 2018.
[28] J. A. Zuclich, D. J. Lund, and B. E. Stuck, "Wavelength dependence of ocular damage thresholds in the near-IR to far-IR transition region: Proposed revisions to MPES," *Health Phys.*, 2007.
[29] M. Takase, Y. Miyake, T. Yamada, T. Tamaki, M. Murakami, and Y. Inoue, "First demonstration of 0.9 µm pixel global shutter operation by novel charge control in organic photoconductive film," *Tech. Dig. - Int. Electron Devices Meet. IEDM*, vol. 2016-Febru, pp. 30.2.1-30.2.4, 2015.
[30] D. Baierl *et al.*, "A hybrid CMOS-imager with a solution-processable polymer as photoactive layer," *Nat. Commun.*, vol. 3, p. 1175, 2012.
[31] S. Sukegawa *et al.*, "A 1/4-inch 8Mpixel back-illuminated stacked CMOS image sensor," *Dig. Tech. Pap. - IEEE Int. Solid-State Circuits Conf.*, vol. 56, no. 1, pp. 484–485, 2013.
[32] R. Breiter *et al.*, "Progress on MCT SWIR modules for passive and active imaging applications," in *Infrared Technology and Applications XLIII*, 2017, vol. 10177, no. May 2017, p. 1017708.
[33] E. J. D. Klem, C. W. Gregory, D. S. Temple, and J. S. Lewis, "Colloidal quantum dot Vis-SWIR imaging: demonstration of a focal plane array and camera prototype (Presentation Recording)," in *Optical Sensing, Imaging, and Photon Counting: Nanostructured Devices and Applications*, 2015, vol. 9555, no. June, p. 955505.
[34] V. Venezia *et al.*, "Second Generation Small Pixel Technology Using Hybrid Bond Stacking," *Sensors*, vol. 18, no. 3, p. 667, Feb. 2018.
[35] Samsung, "Introducing Two New 0.8µm ISOCELL Image Sensors," 2018. [Online]. Available: https://www.samsung.com/semiconductor/insights/news-events/introducing-two-new-0-point-8-micrometer-isocell-image-sensors/. [Accessed: 25-Feb-2019].
[36] J. Maes, N. Castro, K. De Nolf, W. Walravens, B. Abécassis, and Z. Hens, "Size and Concentration Determination of Colloidal Nanocrystals by Small-Angle X-ray Scattering," *Chem. Mater.*, vol. 30, no. 12, pp. 3952–3962, Jun. 2018.
[37] Y. Fang, A. Armin, P. Meredith, and J. Huang, "Accurate characterization of next-generation thin-film photodetectors," *Nat. Photonics*, vol. 13, no. 1, pp. 1–4, 2019.
[38] J. Xu *et al.*, "2D matrix engineering for homogeneous quantum dot coupling in photovoltaic solids," *Nat. Nanotechnol.*, vol. 13, no. 6, pp. 456–462, 2018.
[39] E. Georgitzikis *et al.*, "Optimization of Charge Carrier Extraction in Colloidal Quantum Dots Short-Wave Infrared Photodiodes through Optical Engineering," *Adv. Funct. Mater.*, vol. 28, no. 42, p. 1804502, Oct. 2018.
[40] L. A. A. Pettersson, L. S. Roman, and O. Inganäs, "Modeling photocurrent action spectra of photovoltaic devices based on organic thin films," *J. Appl. Phys.*, vol. 86, no. 1, pp. 487–496, 1999.
[41] H. Gommans, D. Cheyns, T. Aernouts, C. Girotto, J. Poortmans, and P. Heremans, "Electro-optical study of subphthalocyanine in a bilayer organic solar cell," *Adv. Funct. Mater.*, vol. 17, no. 15, pp. 2653–2658, 2007.
[42] C. Hu *et al.*, "The micropatterning of layers of colloidal quantum dots with inorganic ligands using selective wet etching.," *Nanotechnology*, vol. 25, no. 17, p. 175302, May 2014.

Epimitheas Georgitzikis received his diploma in electrical and computer engineering from Aristotle University of Thessaloniki in 2009 (focus in electronics and computer engineering.). He is currently pursuing the Ph.D in Engineering Science in Katholieke Universiteit Leuven, Belgium, under Prof. Paul Heremans dealing with the investigation of the electrical and optical properties of lead-sulfide colloidal quantum dots. On 2016 he joined imec, where he works as a Ph.D researcher on thin-film infrared sensitive photodetectors.

Epimitheas' research has focused on the characterization of thin film semiconductors such as polymers and colloidal quantum dots and their application in novel photodiode detectors.

Pawel E. Malinowski was born in Lodz, Poland, in 1982. He received the M.Sc.Eng. degree in electronics and telecommunications (thesis on design of radiation-tolerant integrated circuits) from the Lodz University of Technology, Poland, in 2006. In 2011, he received the Ph.D. degree in electrical engineering from the KU Leuven, Belgium (thesis on III-nitride-based imagers for space applications).

Pawel is working at imec since 2005, and in the Large Area Electronics Department since 2011. Currently, he is Program Manager "User Interfaces & Imagers" and he focuses on high resolution OLED displays and thin-film image sensors.

Pawel has authored or coauthored more than 30 publications. He was a recipient of the International Display Workshops Best Paper Award in 2014 and the SID Display Week Distinguished Paper Award in 2018.

Yunlong Li received the M.Sc. degree in Engineering from Tsinghua University, Beijing, China in 2002 and the Ph.D. degree in Electrical Engineering from University of Leuven, Belgium in 2007. He is currently a senior R&D engineer at imec, Leuven, Belgium. His current research and development work focus on the integration exploration of novel image sensor technology on top of standard CMOS wafers. He has authored more than 90 papers in peer-reviewed journals and conferences on material, process, integration and reliability in CMOS Back End of Line (BEOL) and 3D-IC Packaging technology.

Jorick Maes received his M.S degree in Chemistry in 2014 from Ghent University of and since September 2014 he is working as assistant in the department of Chemistry at the University of Ghent. Besides teaching, he studies fundamental and applied aspects of semiconductor nanocrystals in the research group of prof. dr. ir. Zeger Hens

Luis Moreno Hagelsieb obtained his PhD in Applied Science at the Université catholique de Louvain, Belgium, emphasizing his work on microelectronic biosensors. Worked in research at the Université catholique de Louvain, focusing its work in biosensors, gas, pressure and optical sensors. He worked in different industrial projects with companies like Samsung, Canberra and vivaMOS, helping in process integration, quality improvement and validation for image and gas sensors. Currently working in the process integration, development and characterization for thin film photodiodes in the IR light applications at IMEC, Belgium.

Stefano Guerrieri was born in Chieti, Italy, in 1973. He received the M.Sc. degree in Solid State Physics (thesis on gate oxide process development on Micron Technology DRAM technologies) from the University of L'Aquila, Italy, in 1999.

From 2000 to 2004, he worked in Applied Materials as System Expert. From 2004 to 2008, Stefano worked in STMicroelectronics central R&D in Agrate Brianza (Milano), Italy, as Process Development Engineer. From 2008 to 2014, he worked in Micron Technology as Process Integration Engineer to develop new Image Sensor Technologies. Since 2014, Stefano has joined IMEC Leuven, Belgium, and he's currently covering the position of Director of the Pixel Technology program.

Stefano has authored or coauthored more than 30 publications on pixel technologies, 3D stacking integration and copper interconnect processes.

Zeger Hens obtained his PhD in 2000 at Ghent University and as FWO postdoctoral fellow he spent 2.5 years with Daniël Vanmaekelbergh in Utrecht University studying electronic properties of semiconductor quantum dots. He is now a full professor at Ghent University, leading the Physics and Chemistry of Nanostructures research group.

Paul Heremans received his PhD degree in electrical engineering in 1990 at the University of Leuven, Belgium, on hot-carrier degradation of MOS transistors. He then joined the optoelectronics group of IMEC, where he worked on optical inter-chip interconnects, and on high efficiency III-V thin-film surface-textured light emitting diodes. His current research interest is oxide and organic electronics, including circuits, backplanes and memories, as well as organic photovoltaics. He is an IMEC Fellow, Director of IMEC's Large Area Electronics department and part-time professor at the Electrical Engineering Department of the University of Leuven.

David Cheyns David Cheyns received his master and Ph.D. in electrical engineering in 2003 and 2008, respectively, from the Katholieke Universiteit Leuven, Belgium. He has over 15 years' experience in thin-film, large-area technologies, and co-authored over 50 publications and 3 patents. He was co-organizer of SPIE Europe, eMRS and member of the scientific advisory board of EUPV-SEC. He pioneered the work on organic tandem solar cells, perovskite materials, OLEDs and thin-film photovoltaic modules at imec. Presently, he is principal scientist and team leader "Future Interactive Thin-film Technology". In this role, he is responsible for the development of the next-generation large-area sensors and actuators for applications such as infrared imaging, gesture recognition, medical imaging, haptic feedback and microfluidics.